

# Mechanism of Fracture in Friction Stir Processed Aluminium Alloy

P. K. Mandal<sup>1</sup>, Mebin T. Kuruvila<sup>2</sup> and Jithin Devasia<sup>3</sup>

<sup>1</sup>Assistant Professor, Department of Metallurgical and Materials Engineering, Amal Jyothi College of Engineering, Koovappally, Kanjirappally, Kerala, INDIA

<sup>2</sup>Assistant Professor, Department of Metallurgical and Materials Engineering, Amal Jyothi College of Engineering, Koovappally, Kanjirappally, Kerala, INDIA

<sup>3</sup>Assistant Professor, Department of Metallurgical and Materials Engineering, Amal Jyothi College of Engineering, Koovappally, Kanjirappally, Kerala, INDIA

<sup>1</sup>Corresponding Author: pkm.iitr@gmail.com

## ABSTRACT

Aluminium alloys are used for important applications in reducing the weight of the component and structure particularly associated with transport, marine, and aerospace fields. Grain refinement by scandium (Sc) addition can eliminate the casting defects and increase the resistance to hot tearing for high strength aluminium alloys. FSP for cast aluminium alloys have been focused and it has great advantages including solid state microstructural evolution, altering mechanical properties by optimizing process parameters. These parameters are tool rotational speeds (720, and 1000 rpm), traverse speeds (80, and 70 mm/min), and axial compressive force at 15 kN, etc. The mechanical properties had been evaluated on FSPed aluminium alloy with different microstructural conditions. Fracture properties of aluminium alloys are very important for industrial applications. Tensile and fracture toughness properties were correlated to microstructural and fractographic features of the aluminium alloys need to explore their essential failure mechanisms.

**Keywords--** Aluminium Alloy, FSP, Fracture Properties, Tensile and Fracture Toughness

## I. INTRODUCTION

The high strength of aluminium alloy is mainly familiar due to age hardening properties. It has wide industrial applications due to their good combination of specific strength, hardness and fracture toughness of this alloy [1, 2]. Main alloying elements of aluminium alloy (7075 series) are Zn and Mg. Thus, Zn/Mg>2 ratio and total Zn+Mg contents (approximately 7 to 8 wt.%) affect the workability of alloys as well as enhance the mechanical properties [3-5]. The aluminium alloys having zinc shows high solubility indicating no lattice distortion for formability point of view and also achieve high strength after accelerating artificial ageing treatment (T<sub>6</sub>). In addition, the degree of hardening achieved depends on the size, number and relative strength of the precipitates. Minor Sc (0.20 wt%) addition in aluminium alloy has been considered a potent grain refining agent because generates numerous precipitation of primary Al<sub>3</sub>Sc particles in the melt, also acting a strong nucleating sites during solidification. According to Kramer et al. (1997) has mentioned that Sc is a powerful grain refiner,

recrystallization inhibitor and dispersoid strengthener. Scandium has potentially refine grains as well as eliminate hot tearing, shrinkage porosity, and reduce precipitation free zones (PFZ) and can inhibit the grain growth by Zener pinning. It has to mentioned that the main strengthening mechanisms are solid solution, age-hardening (coherency strain hardening, chemical hardening, and dispersion hardening), and Sc inoculation effects [6, 7]. In addition, adaptation of friction stir processing (FSP) for cast aluminium alloys have been considered a new surface modification technology which produces the fine recrystallized grains in the stir zone (SZ) due to dynamic recrystallization from SPD, and further improves the mechanical properties. Degree of plastic deformation and heat input are main criteria for FSP created three distinct zones such as SZ, TMAZ, and HAZ exposed by the frictional heat generate between the tool and work piece. FSP has occurred in semi-solid state, typically around 0.6 to 0.7 T<sub>m</sub> (melting temperature) of aluminium alloy [8-10]. It is noted that the alloy has total impurity content (0.34 wt.%) plays in the formation of coarse particles which can serve as the crack initiation sites, and later stages can provide planes of easy crack growth, thereby reducing the deformation capacity of the matrix. FESEM observation of fracture surface revealed several black spots due to Zn vaporization in matrix. SEM observation of the fracture surfaces revealed the multi-mechanism of the fracture process as a competition between several black spots (Zn vaporization) and coarse particles (probably MgZn<sub>2</sub>(η)-phases or Al<sub>3</sub>Sc(L1<sub>2</sub>) coarse particles) and transgranular/intergranular failures in matrix [11]. The transgranular microcrack-induced fracture generated with the formation of black spots in the matrix [12]. The fracture planes have covered with fine dimples, commonly associated with very fine particles. The fracture surfaces are indicated with many fine dimples, representing areas of extensive deformation that preceded the ductile fracture in matrix. Also observed on the walls of large dimples connected with the aggregates of mostly fractured coarse particles/black spots. The places called ridges (2000X), where the cracks may change its direction of propagation that also be identified through FESEM and SEM fractography analysis. It has been mainly focused on metallurgical structures and constitutional variations in relation to their effects on the

toughness and mode of fracture behaviour. The conclusions are to be drawn for this case, the fracture resistance does not simply depend upon the maximum

stress or strain to cause failure but also on the sufficient presence of defects, and coarse particles and their sizes.

## II. EXPERIMENTAL PROCEDURE

Table 1: FSP parameters and tool design.

Tool shoulder diameter (mm)	20
Tool pin diameter (mm)	3
Tool pin height (mm)	3.5
Clockwise and unidirectional tool rotational speeds (rpm)	1000 and 720
Tool traverse speeds (mm/min)	70 and 80
Axial pressure (kN)	15
Tool tilt angle (°)	2.5
Number of passes	two
Plate dimensions	150×90×8 mm <sup>3</sup>

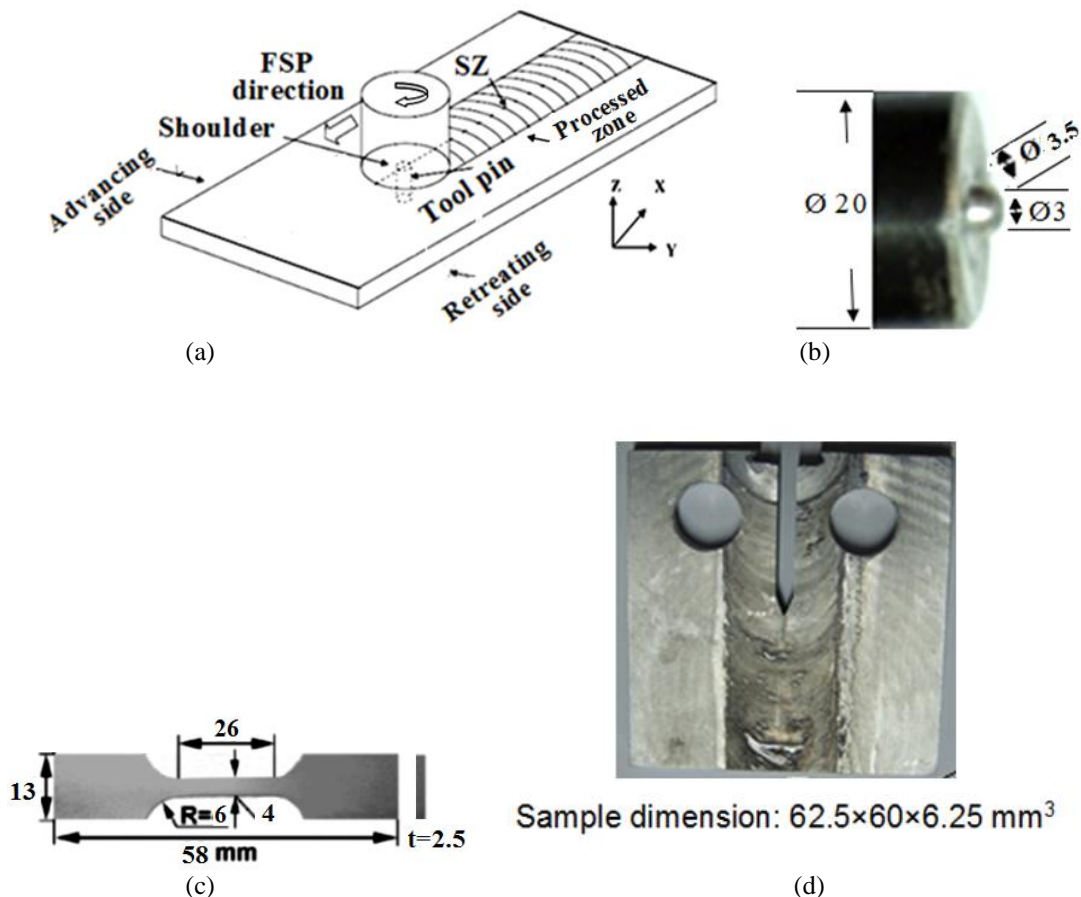


Figure 1: Schematic illustration of (a) FSP set up; (b) Tool pin configuration; (c) Design of tensile test sample (ASTM: E-8/E8-11 sub size); (d) Design of plane-strain fracture toughness ( $K_{IC}$ ) test sample (ASTM: E399)

The nominal composition of the aluminium alloy used in the present study are likely to total solute contents of Zn+Mg=8.86 wt.%, Zn/Mg= 2.02, and Sc used as a grain refiner of 0.45 wt.%, total impurity contents of Si+Fe+Cu+Ni+Sn = 0.34 wt.%, and balance of Al. The alloy was melted and refined in an electrical muffle furnace at 780°C and then poured into a mild steel

metallic mould of rectangular shape with dimensions of approximately 200×90×24 mm<sup>3</sup>. The cast alloy was examined by ICP-AES and AAS analysis. The main plate was sectioned to make it 150×90×8 mm<sup>3</sup> thin sections. The cast plate was subjected to solution treatment at 465°C for 1h and immediate water cooling to room temperature ( $T_4$  heat-treatment). Then,  $T_4$  heat-treated

plate was again subjected to artificial ageing at 140°C for 16h ( $T_6$  heat-treatment) and evaluated for age-hardening effect through Vicker's hardness measurements (average of six indentations) at 1h interval with 10 kg. load and 20s dwell time. Another cast plate was directly subjected to double-pass FSP with specified process parameters as shown in Figure 1(a), then samples collected from processed zone. Each sample was cleaned with acetone then dried and preferred for tensile and fracture toughness testing as per ASTM standard as shown in Figure 1(c-d), respectively. The tensile test was performed on as-cast plate with unidirectional double-pass FSP. The processed samples had been collected from SZ with proper machining and tested by Universal Testing Machine (Model no.: 25 kN, H25 K-S, UK) with cross head speed of 1 mm per min. The tensile test results are shown in Table 2. Another cast plate was subjected to both tensile testing and fracture toughness ( $K_{IC}$ ) testing with specified FSP parameters as shown in Table 3 by Universal Testing Machine (Model no.: 8802) with standard CT specimen of static loading condition. Then, the cast plate after double-pass FSP was notched by CNC Wire Cut Machine (Model no.: Sprintcut 734) made in Japan. The fracture toughness test sample is shown in Figure 1(d), where processed zone depth (3.5 mm) is equivalent to tool pin height. The fracture toughness test was perfectly based on the principle of LEFM and contains three main steps such as generation of crack in the test specimens, measurement of the load at failure stress, and crack depth. In addition, predetermined notch tip crack was generated where crack length is 0.21 mm by Instron testing machine as shown in Table 3. The metallographic studies were examined by Optical microscopy technique, SEM analysis, FESEM and TEM analysis. The samples were cut from the processed zone into small pieces and ground, and then polished with emery papers sequentially from coarser to finer likely to 800, 1000, 1500 and 2000, respectively. Then, cloth polishing was carried out with mechanically rotating wheel using  $Al_2O_3$  slurry until fine scratches removed entirely. The final stage of polishing was done through diamond paste (0.5-1.0  $\mu m$ ) wet by sprayed liquid paraffin oil put on fine cloth by using rotating wheel until to obtain a mirror finish polishing. Then the sample was cleaned with water and dried using a hot air dryer and etched with Keller's reagent (2.5 ml  $HNO_3$  (70%) + 1.5 ml HCl (38%) + 1 ml HF (40%) + 175 ml water). The optical microscope used for this study was a LEICA DMI 5000M (Model no.: Leica Microsystems, Buffalo Grove, IL) microscope. Transmission electron microscopy (TEM) analysis was done for as-cast and artificial aged (140°C for 6h) samples. For TEM analysis, samples were prepared manually by polishing a thin specimen to obtain disk-shaped scratch free surface. At  $10 \times 10 \text{ mm}^2$  disc specimens were thinned down to  $< 0.1 \text{ mm}$ . Finally, 3 mm diameter disc-shaped samples had cut from main polished ( $10 \times 10 \text{ mm}^2$ ) sample which was considered for TEM analysis (Model no.: Techai G<sup>2</sup> 20 S-TWIN at 200 kV). Then, samples were polished using twin-jet electro-polishing with proper solution content to

75%  $CH_3OH$  and 25%  $HNO_3$  at 12 V and -35°C. The tested fracture surfaces had carefully collected from tensile and CT test pieces then cleaned with acetone and preserved in desiccator for further SEM analysis (Model no.: LEO 435VF). Thus, Scanning electron microscopy (SEM) fractography analysis has performed insight into the fracture micromechanisms in the central plane-strain region of the plastic zone.

### III. RESULTS AND DISCUSSION

Development of aluminium alloys on toughness properties have intrinsic mechanisms with crack tip plasticity as the dominating factor. During fracture toughness test the plastic deformation acts as to reduce stress densification at the crack tip by reducing crack tip blunting through the release of dislocations showing ductile behaviour, rather as opposed to local decohesion by simply breaking an atomic bond in brittle behaviour. On the other hand, high strain hardening played major role for ductile fracture as it provides a steady source of hardening to suppress strain hardening localization like necking which in turn creates a wider distribution of damage that microstructurally or distributions of second phases ( $\eta$ ) and  $Al_3Sc$  particles again provide greater resistance to fractures. The  $MgZn_2$  ( $\eta$ ) is the major precipitate in high strength aluminium alloys. The solid solubility of  $MgZn_2$  phases in Al-Zn-Mg alloy reduces significantly when the temperature varies from eutectic point to room temperature. The artificial ageing treatment can precipitate nano-sized particles that contain the mixture of GP zones,  $\eta$ ,  $\eta'$ , and  $Al_3Sc$  for faster ageing effects. These precipitates have a strong precipitation strengthening, prevent the movement of dislocations and help in increasing the strength as the dislocation pile-up, further shear mechanism or bypass mechanism (Orowan strengthening) become active [13]. For these mechanisms an additional stress is required to move the dislocation in slip plane to increases yield strength in matrix. Figure 2 shows TEM micrograph with SAD pattern of as cast inhomogeneity with dendritic morphology in matrix. The  $Al_3Sc$  particles embedded in matrix, precipitates on grain boundaries (indicated by red arrows), and dislocations are seems to be generated on the grain boundaries, and SAD pattern exhibits uniform precipitates in matrix. Figure 3 shows TEM micrograph with SAD pattern for  $T_6$  alloy which shows refined grains and needle shape of  $\eta'$  phases,  $Al_3Sc$  particles (indicated by red arrows), and tangle of dislocations specially on the grain boundaries. The  $\eta'$  is the main age-hardening phase for this alloy. The hardness value is 164 HV (10 kg. load) for this 6h ageing stage. Figure 4 shows optical microstructure of AC+FSP alloy exhibiting mainly two distinct regions such as stir zone (SZ) and thermomechanically affected zone (TMAZ), in which SZ is the finer region causes dynamic recrystallization [14] or grain growth may slow due to the presence of fine precipitates,  $Al_3Sc$  in the matrix and TMAZ is prone to cracks generated due to torsional

effects (indicated by red arrows). The black arrows indicate several pits which possibly due to Zn vaporization effects. The high rotational speed at 1000

rpm and traverse speed at 70 mm/min have momentarily generated high frictional heat of 400–500°C in SZ probably due to caused of these defects [15, 16].

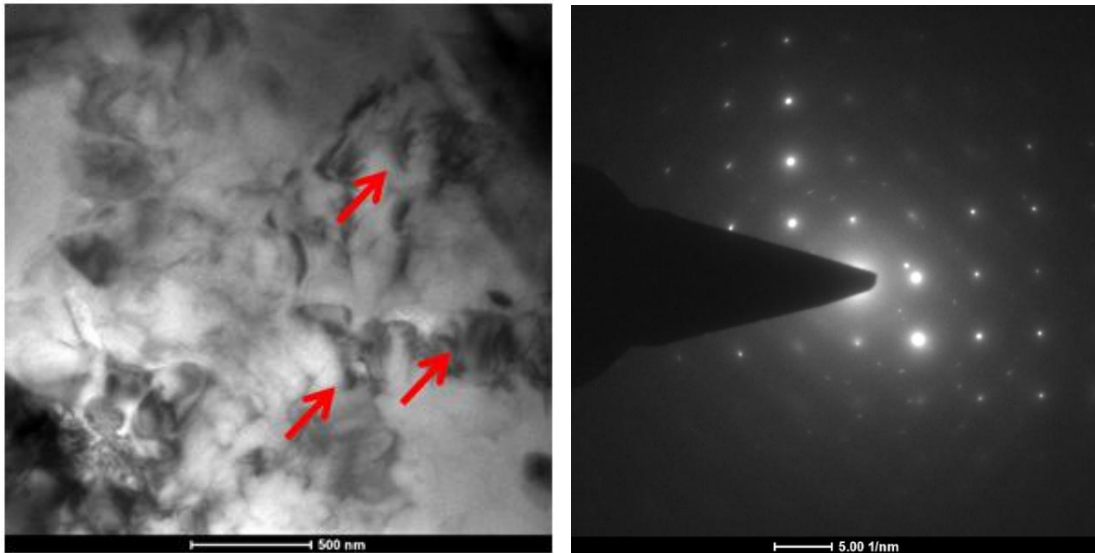


Figure 2: TEM microstructure with SAD pattern of AC (as cast) aluminium alloy

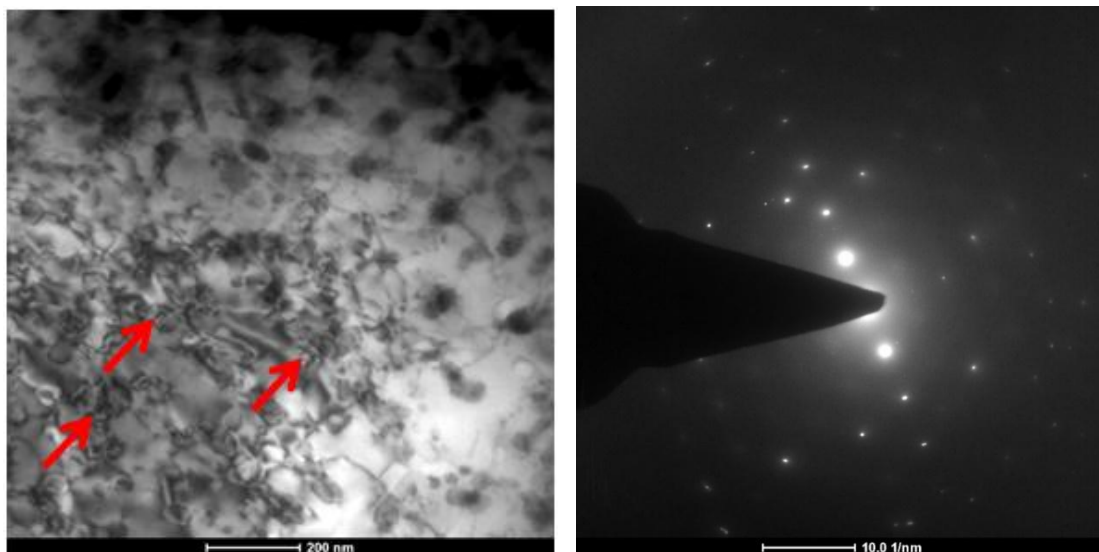


Figure 3: TEM microstructure with SAD pattern of aluminium alloy at  $T_6$  (140°C for 6h) condition

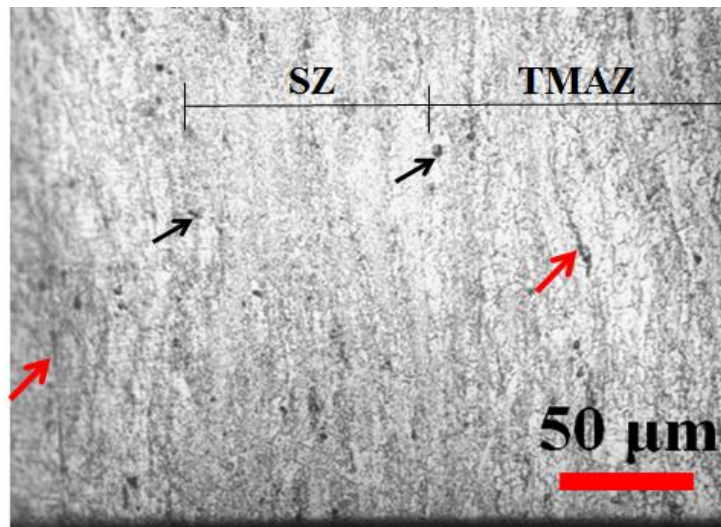


Figure 4: Optical microstructure of aluminium alloy at AC+FSP condition. (1000 rpm and 70 mm/min)

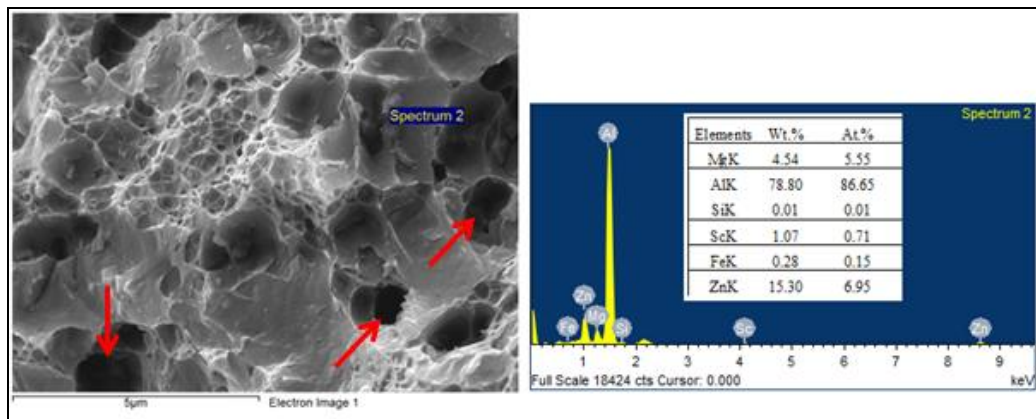


Figure 5: FESEM microstructure with EDS analysis of aluminium alloy at AC+FSP condition. (1000 rpm and 70 mm/min)

Figure 5 shows FESEM microstructure with EDS analysis which red arrows indicate dip holes probably generate cracks at these points on the tensile loading condition. The spot of EDS analysis confirm Zn contents of 15.3 wt.% and Sc contents of 1.07 wt.%. Figure 6 shows SEM tensile fractographs at different magnifications of aluminium alloy at AC+FSP condition, in which low magnification (200X) fractography exhibits continuous network of ductile fracture but steadiness break due to sudden creation of dip holes probably due to cause of defects like Zn vaporization or coarse precipitates ( $\text{Al}_3\text{Sc}$  or Fe, Si -impurities). It is clearly indicated in high magnification (2000X) fractography which revealed that the cracks generate in transgranular manner, with several dip holes (indicated by red arrows) due to coarse precipitates. Figure 7 shows SEM compact-tension (CT) fractographs at different magnifications of aluminium alloy at AC+FSP condition, in which low magnification (500X) fractography exhibits very fine ductile mode of fracture surface but steadiness break due to sudden dip cracks (indicated by red arrows) perhaps due to caused of Zn vaporization points or coarse particles [17]. It has to mentioned that the two different types of fracture mode (for tensile test 1000 rpm, 70

mm/min and for toughness test 720 rpm, 80 mm/min) exhibit dissimilar types of feature of fracture surfaces. Also, similar type of fracture mode is exhibited in the case of high magnification fractography (2000X), where sudden dip holes are clearly visible with different ridges formation along several micro-voids. Table 2 shows mechanical properties of aluminium alloy after AC+FSP condition, which is exhibited higher 0.2% proof strength of 159 MPa, UTS of 283 MPa, elongation of 8%, and Vicker's hardness along the SZ of 146HV, respectively. It is to combined contribution of elimination of as-cast inhomogeneity and porosities, fine distribution of hardening precipitates of  $\eta$  and  $\text{Al}_3\text{Sc}$  particles in the processed zone. FSP parameters of 720 rpm and 80 mm/min traverse speed exhibited better fracture toughness ( $K_{IC}$ ) value of 32  $\text{MPa}\sqrt{\text{m}}$  for aluminium alloy perhaps due to lower heat input (ratio of 720/80=9) (Table 3) [18-20]. The important microstructural parameters governing the toughness properties are the resistance of these hardening particles, and their interfaces to cleavage and decohesion, the size and local distribution of active particles. The matrix plastic deformation behaviour is itself a function of work hardening and the flow stress, which directs

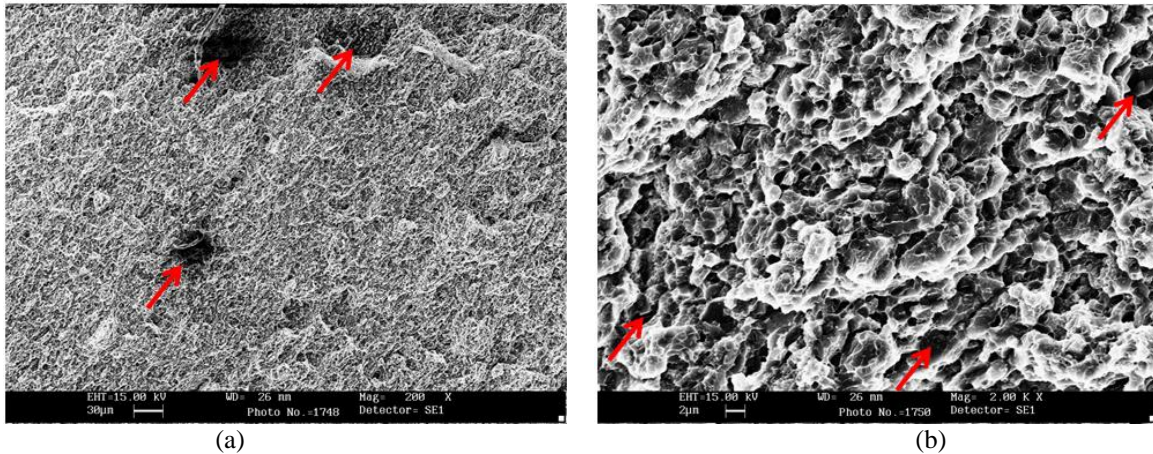


Figure 6: SEM tensile fractographs of aluminium alloy at AC+FSP condition: (a) low magnification (200X), (b) high magnification (2000X). (1000 rpm and 70 mm/min)

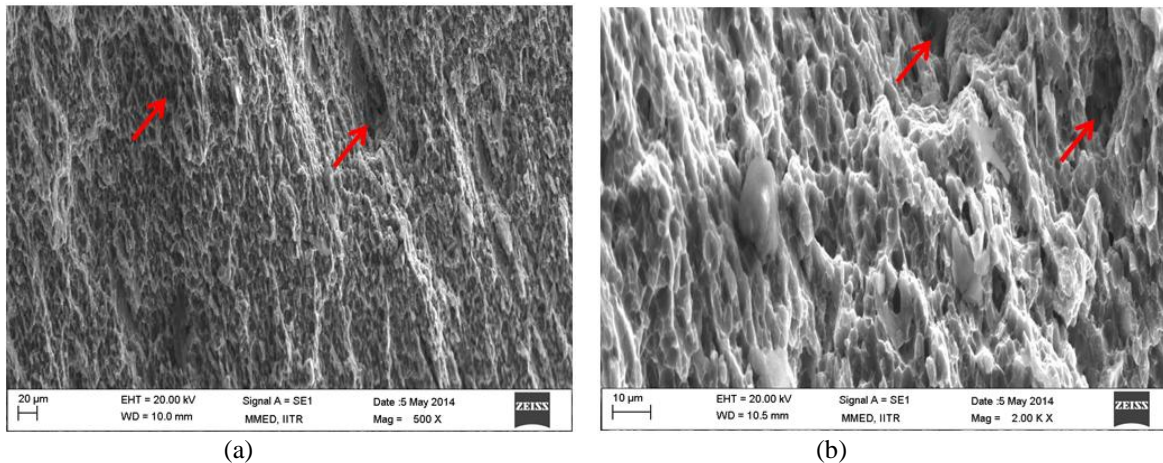


Figure 7: SEM Compact-tension (CT) fractographs of aluminium alloy at AC+FSP condition: (a) low magnification (500X), (b) high magnification (2000X). (720 rpm and 80 mm/min)

the build-up of local strain concentrations leading to initiation as well as the subsequent linking-up process. FSP for tensile tests had been carried out for two different parameters such as 1000 rpm and 70 mm/min traverse speed (i.e., heat input = 1000/70 = 14.3), and 720 rpm and 80 mm/min traverse speed (i.e., heat input = 720/80 = 9), respectively [21-23]. When heat input is less (i.e., 9) then the tensile properties dramatically have been

changed for 0.2% proof strength increase to 13%, UTS increase to 13.4%, elongation increase to 12.5%, respectively. It is concluded that the FSP parameters have played important role for enhancement of mechanical properties as well as fracture toughness due to minimizing of defects like Zn vaporization, coarsening of impurity particles, and fine precipitates distribution which arrest the cracks on the tip of notch.

Table 2: Mechanical properties after double-pass FSP.

7075 Al Alloy	FSP parameters	AC+FSP condition			
		$\sigma_{0.2}$ (MPa)	$\sigma_u$ (MPa)	$\delta$ (%)	HV <sub>10kg.</sub>
	1000/70	159	283	8	146

Table 3: The following parameters have been selected during tensile test and plane-strain fracture toughness test.

7075 Al Alloy	FSP Parameters (rpm/traverse speed)	Applied load (in N)	Experimental parameters and consequent results								
			R ratio	$\sigma_{0.2}$ (MPa)	$\sigma_u$ (MPa)	$\delta$ (%)	Y. Modulus (MPa)	Frequency (f) (Hz)	No. of cycles have yielded during pre-crack stage	Crack length generated (mm)	K <sub>IC</sub> value (MPa√m)

	AC+FSP and 720/80	800	0.1	180	321	9	$6 \times 10^4$	2	1200	0.21	32

#### IV. CONCLUSIONS

Many investigations have been reported till now on the strength of aluminium alloys and their fracture behaviour. The revelation of fracture characteristics of aluminium alloy was influenced by various metallurgical factors such as grain size, precipitates distribution and size which depend upon the total solute contents and their ratio, scandium effects, and plastic deformation by FSP. The following results are obtained below:

(1) Minor scandium (>0.20 wt%) addition can refine grains, eliminate hot tearing and precipitation free zone (PFZ) in cast aluminium alloys.

(2) T<sub>6</sub> heat treatment (140°C for 6h) can precipitate nano-sized particles that contain the mixture of GP zones, η, η<sub>1</sub>, and Al<sub>3</sub>Sc for faster ageing effects.

(3) TEM with SAD investigation revealed that the as-cast inhomogeneities, existence of Al<sub>3</sub>Sc particles, seems to dislocation generation on the grain boundaries, and FESEM with EDS analysis revealed defects like dip holes in the matrix.

(4) FSP is a novel solid state surface modification technology and resultant microstructures implies fine grains due to SPD and dynamic recrystallization mechanism.

(5) It has to be mentioned that the presence of impurity elements (0.34 wt.%) differ the fracture mechanism and their interrelationship of cracking path and distribution of such impurities during FSP. The coarse impurities are detrimental to their ductility and fracture toughness.

(6) In this study, the two different types of fracture mode have been investigated such as tensile test at rotational speed of 1000 rpm, traverse speed of 70 mm per min and fracture toughness (K<sub>IC</sub>) test for 720 rpm, 80 mm/min which exhibited dissimilar types of feature of fracture surfaces. In case of FSP parameters of 720 rpm and 80 mm/min exhibited better tensile and fracture toughness properties of aluminium alloy.

(7) FESEM and SEM examination of fracture surfaces can help in understanding of mechanical properties as well as complex interactions between the fracture micromechanisms and the variation of parameters with alloy chemistry and their impurity level.

#### REFERENCES

[1] Afify, N., Gaber, A-F., & Abbady, G. (2011). Fine scale precipitations in Al-Zn-Mg alloys after various aging temperatures. *Materials Sciences and Applications*, 2, 427-434.

[2] Han, N.M., Zhang, X.M., Liu, S.D., He, D.G., & Zhang, R. (2011). Effect of solution treatment on the strength and fracture toughness of aluminium alloy 7050. *Journal of Alloys and Compounds*, 509, 4138-4145.

[3] Loffler, H., Kovacs, I., & Lendvai, J. (1983). Review decomposition processes in Al-Zn-Mg alloys. *Journal of Materials Science*, 18, 2215-2240.

[4] Engdahl, T., Hansen, V., Warren, P.J., & Stiller, K. (2002). Investigation of fine scale precipitates in Al-Zn-Mg alloys after various heat treatments. *Materials Science and Engineering, A* 327, 59-44.

[5] Priya, P., Johnson, D.R., & M.J.M. Krane. (2017). Modeling phase transformation kinetics during homogenization of aluminium alloy 7050. *Computational Materials Science*, 138, 277-287.

[6] Costa, S., Puga, H., Barbosa, J., & Pinto, A.M.P. (2012). The effect of Sc addition on the microstructure and age hardening behaviour of as cast Al-Sc alloys. *Materials and Design*, 42, 347-352.

[7] Mandal, P.K. (2017). Heat treatment and friction stir processing effects on mechanical properties and microstructural evolution of sc inoculated Al-Zn-Mg alloys. *Materials Science and Metallurgy Engineering*, 4(1), 16-28.

[8] Nascimento, F., Santos, T., Vilaca, P., Miranda, R.M., & Quintino, L. (2009). Microstructural modifications and ductility enhancement of surfaces modified by FSP in aluminium alloys. *Materials Science and Engineering A*, 506, 16-22.

[9] Kurt, A., Uygur, I., & Cete, E. (2011). Surface modification of aluminium by friction stir processing. *Journal of Materials Processing Technology*, 313-317.

[10] Ku, M-H., Hung, F-Y., Lui, T-S., Chen, L-H., & Chiang, W-T. (2012). Microstructural effects of Zn/Mg ratio and post heat treatment on tensile properties of friction stirred process (FSP) Al-xZn-yMg alloys. *Materials Transactions*, 53(5), 995-1001.

[11] Vratnica, M., Cvijovic, Z., & Radovic, N. (2008). The effect of compositional variations on the fracture toughness of 7000 al-alloys. *Materials and Technology*, 42(5), 191-196.

[12] Mandal, P.K. (2017 June). Investigation of microstructure and mechanical properties of Al-Zn-Mg and Al-Zn-Mg-Sc alloys after double passes friction stir processing. *International Journal of Materials Science and Engineering*, 5(2), 47-59.

[13] Zhenbo, H., Zhimin, Y., Sen, L., Ying, D., & Baochuan, S. (2010 Aug). Preparation, microstructure and properties of Al-Zn-Mg-Sc alloy tubes. *Journal of Rare Earths*, 28(4), 641-646.

- [14] Gholami, S., Emadoddin, E., Tajally, M., & Borhani, E. (2015). Friction stir processing of 7075 Al alloy and subsequent aging treatment. *Transactions of Nonferrous Metals Society of China*, 25, 2847-2855.
- [15] Lin, F.C. & Ma, Z.Y. (2009). Achieving high strain rate superplasticity in cast 7075Al alloy via friction stir processing. *Journal of Materials Science*, 44, 2647-2655.
- [16] Hamilton, C., Sommers, A., & Dymek, S. (2009). A thermal model of friction stir welding applied to Sc-modified Al-Zn-Mg-Cu alloy extrusions. *International Journal of Machine Tools & Manufacture*, 49, 230-238.
- [17] Yen, A., Chen, L., Liu, H.S., Xiao, F.F., & Li, X.Q. (2015). Study the strength and fracture toughness of al-zn-mg-cu-ti(-sn) alloys. *Journal of Mining and Metallurgy Section B: Metallurgy*, 51(1), B, 73-79.
- [18] Fuller, C.B., Krause, A.R., Dunand, D.C., & Seidman, D.N. (2002). Microstructure and mechanical properties of a 5754 aluminium alloy modified by Sc and Zr additions. *Materials Science and Engineering A*, 338, 8-16.
- [19] Kamp, N., Sinclair, I., & Starink, M.J. (2002 Apr). Toughness-strength relations in the overaged 7449 Al-based alloy. *Metallurgical and Materials Transactions A*, 33A, 1125-1136.
- [20] Seah, K.H.W. & Sharma, S.C. (1996). Fracture toughness of cast Al-Zn-Mg alloys. *Journal of Materials Science and Technology*, 12, 199-202.
- [21] Ludtka, G.M. & Laughlin, D.E. (1982 Mar). The Influence of Microstructure and Strength on the Fracture Mode and Toughness of 7XXX Series Aluminium Alloys. *Metallurgical and Materials Transactions A*, 13A, 411-425.
- [22] Fukui, T. (1974). Influence of iron and silicon on toughness and fracture characteristics of Al-Mg-Mn and Al-Zn-Mg alloys. *Transactions of The Japan Institute of Metals and Materials (JIM)*, 15, 1-10.
- [23] Reddy, A.C. & Rajan, S.S. (2005 Feb). Influence of ageing, inclusions and voids on ductile fracture mechanism in commercial Al-alloys. *Bulletin of Material Science*, 28(1), 75-79.